Author Manuscript

NEUVAC: Nonlinear Extreme Ultraviolet Irradiance Model for Aeronomic Calculations

Brandt, Daniel A.[1] **and Ridley, Aaron J.**[2]

[1]Michigan Tech Research Institute - Michigan Technological University, Ann Arbor, MI, USA
[2]Department of Climate and Space Sciences and Engineering, University of Michigan, Ann Arbor, MI USA

Key Points:

- NEUVAC, a new empirical model of solar extreme ultraviolet irradiance based on FISM2, is presented.
- The model performance is compared to outputs from EUVAC, HEUVAC, and HFG.
- The model quantifies uncertainty in a manner compatible with global atmospheric models.

Corresponding author: Daniel A. Brandt, daabrand@mtu.edu

This is the author manuscript accepted for publication and has undergone full peer review but has not been through the copyediting, typesetting, pagination and proofreading process, which may lead to differences between this version and the Version of Record. Please cite this article as doi: 10.1029/2024SW004043.

This article is protected by copyright. All rights reserved.

Author Manuscript

Abstract

The need for reliable estimates of solar extreme ultraviolet (EUV) for operational space weather nowcasting and forecasting has motivated the development of new model of solar irradiance variability in 59 wavelength bins between 1 and 1750 Å. The model employs a nonlinear parameterization of rebinned daily FISM2 irradiances and is termed NEUVAC: Nonlinear Extreme Ultraviolet Irradiance Model for Aeronomic Calculations. The model is parameterized in terms of F10.7 and 54-day averaged F10.7 in a backwards-looking window. The model takes advantage of the high accuracy and resolution of FISM2, and the consistent availability of F10.7 data in order to provide the space weather community with an empirical irradiance model that requires only two inputs, and is applicable for solar EUV forecasting. Additionally, the model is capable of running ensembles and providing estimates of quantified uncertainty for usage by downstream ionosphere-thermosphere models. The model is evaluated against native FISM2 outputs in the 37 bins used by the EUVAC model, as well as the bins specified by Solomon and Qian. Its accuracy and precision is also compared to that of EUVAC, HEUVAC, and the HFG models.

Plain Language Summary

NEUVAC, a new empirical model of solar extreme ultraviolet (EUV) irradiance is presented. The model represents solar EUV irradiance in 59 wavelength bins between 1 and 1750 Å, and is constructed between F10.7, 54-day averaged F10.7 in a backwards-looking window, and binned estimates of solar irradiance provided by the FISM2 model. NEUVAC is evaluated against FISM2 and compared with other empirical models such as EUVAC, HEUVAC, and the HFG models.

1 Introduction

Solar EUV irradiance plays a dominant role in modulating the temperature, density, and composition of the terrestrial upper atmosphere (H. Hinteregger, 1981; Hedin & Mayr, 1987; Anderson & Hawkins, 2016). Due to the effects of solar EUV on the atmospheric density in particular, the space weather community requires accurate estimates of the solar EUV in order to carry out space situational awareness and for conducting satellite collision avoidance (Bussy-Virat et al., 2018). Though measurements of the solar EUV spectrum began in the 1970s with the advent of the AE satellites (H. Hinteregger et al., 1976) and were succeeded by the SUSIM instrument aboard the Upper Atmospheric Research Satellite (UARS) in the 1990s (Brueckner et al., 1993), it has only been following the success of missions such as TIMED/SEE (Woods et al., 2000), SORCE/SOLSTICE (Rottman, 2005), and SDO/EVE (Woods et al., 2012) that consistent and reliable measurements of the solar EUV spectrum have been available. These successes notwithstanding, satellite instrument degradation issues that have necessitated the conducting of regular calibrations - often with the aid of rocket measurements (Woodraska et al., 2004) - have hampered the fidelity of the satellite measurements. As a result, the community has continuously relied on solar proxies strongly correlated with solar EUV irradiance in order to generate operational predictions of the atmospheric state. Some of these proxies include the F10.7 solar index (Tapping, 2013), the Mg-II core-to-wing ratio (Viereck et al., 2004), Lyman-α (Machol et al., 2019), Ca-II K line emissions (Bertello et al., 2010), and the revised sunspot number (Clette & Lefèvre, 2016). Since no proxy in particular has yet been shown to satisfactorily capture the various modes of temporal variability throughout the entire solar EUV spectrum (de Wit et al., 2008), various empirical models have been developed between multiple solar proxies and the binned solar EUV spectrum.

This article is protected by copyright. All rights reserved.

Author Manuscript

These models include the well-known EUVAC model (P. Richards et al., 1994; Schunk & Nagy, 2009), which consists of linear fits between F10.7 and 81-day averaged F10.7 (hereafter referred to as F10.7A) and the F74113 solar EUV reference spectrum obtained by a rocket experiment (Heroux & Hinteregger, 1978). EUVAC returns solar fluxes across 37 wavelength bins between 5 and 105 nm. EUVAC was succeeded by the HEUVAC model, which introduced variable wavelength resolution and extended wavelength coverage to below 5 nm (P. G. Richards et al., 2006). Another widely-used approach uses the SC21REFW reference spectrum and scaling factors obtained from the Atmospheric Explorer (AE) program and associated rocket measurements by H. E. Hinteregger et al. (1981) (HFG). The HFG model parameterizes the solar EUV flux in 22 variable-width wavelength bins at coarse resolution (Solomon & Qian, 2005), and enables improved calculations of altitude-dependent energy deposition into the thermosphere. Other paradigms include SOLAR2000, which parameterizes solar irradiance between 1 and 1,000,000 nm in terms of the novel E10.7 proxy, which is the time-dependent, integrated solar EUV flux at the top of the Earth's atmosphere (Tobiska et al., 2000), the NRLEUV2 model, which parameterizes the quiet solar spectrum based on CDS and SUMER spectrometer measurements aboard SOHO (Warren, 2006), the Girazian and Withers (2015) empirical model, which parameterizes TIMED/SEE irradiance as a function of the average of daily F10.7 and F10.7A, and the GOES-R EUVS model developed by the National Oceanic and Atmospheric Administration (NOAA), which models solar EUV irradiance in twenty-two 5 nm wide intervals from 5 nm to 115 nm, and one 10 nm wide interval from 117 to 127 nm (Thiemann et al., 2019).

The Flare Irradiance Spectrum Model (FISM), has seen particular success due to highly accurate modeling of solar EUV irradiance between 0 and 190 nm through parametric modeling of daily and flare-related irradiance based on multiple solar proxies and satellite measurements. The first version of the model (FISM1) achieved high-fidelity estimates of solar EUV irradiance in wavelength bins from 0.1 nm to 190 nm at 1 nm wavelength resolution by modeling a long-term variations away from the solar minimum reference spectrum due to the solar rotation, adjusting daily values in each bin based on the strength of individual solar proxies in affecting changes of irradiance in that bin, and individually modeling the impulsive and gradual phases of solar flares. FISM thus contains a daily component (Chamberlin et al., 2007) and a flare component (Chamberlin et al., 2008). FISM2 improved upon FISM1 by modeling irradiance between 0.5 to 1899.5 nm at 0.1 nm wavelength resolution, through the inclusion of measurements from newer instruments such as SDO/EVE, SORCE/XPS (Woods & Rottman, 2005), and SORCE/SOLSTICE (Chamberlin et al., 2020). Due to the fact that FISM2 uses 108-day smoothed proxies to generate estimates of irradiance on a given date, it is limited for near-real-time applications, where the previous 54 days, plus whatever days after that are available, are used.

Even with the numerous modeling paradigms previously mentioned, the space weather community has continued to rely on proxies in operational situations; atmospheric models that see widespread use by the community, including the NCAR Thermosphere-Ionosphere-Electrodynamics General Circulation Model (TIE-GCM) (Qian et al., 2014), the Coupled Thermosphere Ionosphere Plasmasphere Electrodynamics Model (CTIPe) (Codrescu et al., 2012), The Whole Atmosphere Community Climate Model (WACCM) (Liu et al., 2018), the Whole Atmosphere Model-Ionosphere Plasmasphere Electrodynamics Forecast System (WAM-IPE) (Akmaev et al., 2008; Maruyama et al., 2016; Zhan et al., 2024), and the International Reference Ionosphere (IRI) (Bilitza et al., 2022) all use either F10.7 directly, or use the EUVAC, HEUVAC, or HFG models driven by F10.7 to estimate EUV input into the upper atmosphere. This has necessitated the development of robust methods for ensuring continuous coverage of solar proxies during outages (Elvidge et al., 2023), and the success of the FISM2 model in particular as well has led to the development of entirely data-driven statistical approaches for forecasting future values of the irradiances with quantified uncertainties (Brandt et al., 2024). The reliance on proxies alone, how-

This article is protected by copyright. All rights reserved.

Author Manuscript

ever, is not ideal, since each each proxy has its own limitations in describing the solar EUV variations on different time scales (Dudok de Wit et al., 2009; Y. Chen et al., 2011). The space weather community has therefore made it clear that estimates of EUV irradiance itself are ideal for nowcasting and forecasting (Vourlidas & Bruinsma, 2018). In the case of FISM2, reliance on future data to make an estimate of irradiance at the present can limit the utility of nowcasts and forecasts, and an approach is needed that captures FISM2's accuracy but relies only on historical information.

In order to respond to this need, we present NEUVAC: Nonlinear Extreme Ultraviolet Irradiance Model for Aeronomic Calculations. NEUVAC is an empirical model of the EUV irradiance that uses nonlinear fits between F10.7, 54-day averaged F10.7 in a backwards window (hereafter referred to as F10.7B), and rebinned FISM2 irradiance. The model uses F10.7 as the only input due to its regular availability and ease of measuring from the ground, and reconstructs FISM2 irradiances since those irradiances themselves represent the community standard for EUV estimates, given that they are generated with the aid of direct measurements of EUV from several satellite missions. In relying on only F10.7 and F10.7B, NEUVAC uses only a single proxy and does not rely on future estimates of that proxy in order to perform nowcasting. Additionally, given a suitable means of forecasting F10.7, such as with flux transport(Henney et al., 2012, 2015), EUV forecasts can be obtained for operational use. NEUVAC generates EUV irradiance estimates in the 59 wavelength bins between 0.1 and 175 nm used in the Global Ionosphere Thermosphere Model (GITM) (Ridley et al., 2006). These bins are an expansion of the 37 EUVAC bins, extending to both higher and lower energies, which allows energy deposition into the mesosphere, where CO_2 and NOx chemistry are important in the energy balance of the atmosphere. NEUVAC also provides uncertainty quantification derived from normalized bin-wise correlations of residuals with respect to FISM2. The model construction enables the generation of ensembles of irradiance estimates. Model performance is evaluated against native FISM2 outputs to assess accuracy, and compared with EUVAC, HEUVAC, and the HFG models.

2 Methodology

2.1 Irradiance Data

The fitting of NEUVAC itself was performed between F10.7, F10.7B and FISM2 rebinned into the 59 wavelength bins used by GITM. In order to compare NEUVAC and FISM2 to EUVAC and HEUVAC, selection of certain bands must be done. EUVAC and HEUVAC cover a smaller range of wavelengths than FISM2 and NEUVAC, so only the corresponding 37 bands between the rebinned FISM2 data, the NEUVAC outputs, and the native EUVAC/HEUVAC outputs are compared. These 37 bins can be found below in Table 1, and we refer to them henceforth as the 'EUVAC bins'. The parameters for the EUVAC model were taken from Table 1 of (P. Richards et al., 1994), and the parameters for HEUVAC were directly provided by Phil Richards. The EUVAC model employs a simple scaling method according to the following formula:

$$f(\lambda) = f_{\text{ref}}(\lambda)\,[1 + A(\lambda)\,(P - 80)], \tag{1}$$

where f_{ref} is the binned reference spectrum, A is a scale factor, and $P = (F10.7 + F10.7A)/2$.

This article is protected by copyright. All rights reserved.

Author Manuscript

Table 1: Parameters for the EUVAC model.

Lower Boundary (Å)	Upper Boundary (Å)	Bin Center (Å)	EUVAC f_{ref} (F74113)	A_i
50	100	75	1.200	1.0017e-02
100	150	125	0.450	7.1250e-03
150	200	175	4.800	1.3375e-02
200	250	225	3.100	1.9450e-02
		256.3	0.460	2.7750e-03
		284.15	0.210	1.3768e-02
250	300	275	1.679	2.6467e-02
		303.31	0.800	2.5000e-02
		303.78	6.900	3.3333e-03
300	350	325	0.965	2.2450e-02
		368.07	0.650	6.5917e-03
350	400	375	0.314	3.6542e-02
400	450	425	0.383	7.4083e-03
		465.22	0.290	7.4917e-03
450	500	475	0.285	2.0225e-02
500	550	525	0.452	8.7583e-03
		554.37	0.720	3.2667e-03
		584.33	1.270	5.1583e-03
550	600	575	0.357	3.6583e-03
		609.76	0.530	1.6175e-02
		629.73	1.590	3.3250e-03
600	650	625	0.342	1.1800e-02
650	700	675	0.230	4.2667e-03
		703.36	0.360	3.0417e-03
700	750	725	0.141	4.7500e-03
		765.15	0.170	3.8500e-03
		770.41	0.260	1.2808e-02
		789.36	0.702	3.2750e-03
750	800	775	0.758	4.7667e-03
800	850	825	1.625	4.8167e-03
850	900	875	3.537	5.6750e-03
900	950	925	3.000	4.9833e-03
		977.02	4.400	3.9417e-03
950	1000	975	1.475	4.4167e-03
		1025.72	3.500	5.1833e-03
		1031.91	2.100	5.2833e-03
1000	1050	1025	2.467	4.3750e-03

Note: The FISM2 data were rebinned into these bins before performing the fits for NEUVAC. HEUVAC outputs were also distributed in these bins for comparisons. The fourth column gives the F74113 reference fluxes ($\times 10^{-9}$ photons cm^{-2} s^{-1}), while the fifth column gives the factor $A(\lambda)$ for scaling the F74113 fluxes. The turquoise rows indicate the singular wavelength emission lines in the model. Read 1.0017e-02 as 1.0017×10^{-2}.

In addition to the above comparisons, we also performed comparisons in the Solomon and Qian bins (Table 2) (referred to henceforth as the b22 bins). The scaled spectrum for the HFG model in the b22 bins is given by the following formula:

This article is protected by copyright. All rights reserved.

Author Manuscript

$$f(\lambda) = f_{\text{ref}}(\lambda) + r_1 c_1(\lambda) + r_2 c_2(\lambda), \tag{2}$$

where f_{ref} is binned reference spectrum, c_k are the contrast ratios in Table 2, and

$$\begin{aligned} r_1 &= 0.0138\,(F10.7 - 71.5) + 0.005\,(F10.7 - F10.7A + 3.9) \\ r_2 &= 0.5943\,(F10.7 - 71.5) + 0.381\,(F10.7 - F10.7A + 3.9)\,. \end{aligned} \tag{3}$$

FISM2 outputs are directly obtainable in the b22 bins, so no rebinning is required. We then performed the fitting for NEUVAC again between F10.7, F10.7B and FISM2 in the b22 bins and made comparisons to the b22 bins corresponding to EUVAC and HFG models.

For the sake of brevity, in the rest of this paper, we will use 'NEUVAC-59' to refer to the standard NEUVAC model in the GITM bins, of which the 37 EUVAC bins are a subset. We will use 'NEUVAC-37' when displaying NEUVAC results in the 37 EUVAC bins. We will use 'EUVAC' and 'HEUVAC-37' to describe those models in the 37 EUVAC bins, while we will use 'NEUVAC-22' to describe the NEUVAC model in the Solomon bins and 'EUVAC-22' to describe the EUVAC model in the b22 bins. We will simply use 'HFG' to describe the model of H. E. Hinteregger et al. (1981) based off of the SC21REFW reference spectrum. Coefficients for EUVAC-22 and HFG can be found in Table A1 of Solomon and Qian (2005), and are replicated in Table 2. When referring to binning schemes, we will use 'b59' to refer to the 59 bins used by GITM and 'b37' to refer to the EUVAC bins. A schematic of the corresponding wavelength coverage in the EUVAC bins and the Solomon bins can be found in Figure 1.

Table 2: The b22 bins, including parameters for EUVAC-22 and HFG. NEUVAC-22 was fit to FISM2 data in these bins, and afterwards was compared to EUVAC-22 and HFG. Overlapping bins are in light gray.

Lower Boundary (Å)	Upper Boundary (Å)	Bin Center (Å)	HFG f_{ref}	HFG c_1	HFG c_2	EUVAC f_{ref}	EUVAC A
0.5	4	2.25	5.010e+01	0.000e+00	2.948e+02	5.010e+01	6.240e-01
4	8	6	1.000e+04	0.000e+00	7.6000e+03	1.000e+04	3.710e-01
8	18	13	2.000e+06	0.000e+00	4.6000e+05	2.000e+06	2.000e-01
18	32	25	7.600e+06	7.470e+05	9.220e+05	2.850e+07	6.247e-02
32	70	51	1.659e+08	6.623e+07	4.293e+06	5.326e+08	1.343e-02
70	155	112.5	4.012e+08	1.662e+08	5.678e+06	1.270e+09	9.182e-03
155	224	189.5	2.078e+09	1.510e+08	6.273e+07	5.612e+09	1.433e-02
224	290	257	1.724e+09	3.310e+08	9.834e+07	4.342e+09	2.575e-02
290	320	305	6.793e+09	2.220e+09	4.286e+07	8.380e+09	7.059e-03
320	540	430	2.750e+09	5.469e+08	1.080e+08	2.861e+09	1.458e-02
540	650	595	5.035e+09	2.969e+09	1.590e+07	4.830e+09	5.857e-03
650	798	724	1.562e+09	6.938e+08	8.208e+06	1.459e+09	5.719e-03
650	798	724	1.264e+09	6.690e+08	5.445e+05	1.142e+09	3.680e-03
798	913	855.5	3.011e+09	3.011e+09	0.000e+00	2.364e+09	5.310e-03
798	913	855.5	4.661e+09	4.213e+09	0.000e+00	3.655e+09	5.261e-03
798	913	855.5	1.020e+09	1.020e+09	0.000e+00	8.448e+08	5.437e-03
913	975	944	5.441e+08	4.187e+08	0.000e+00	3.818e+08	4.915e-03
913	975	944	1.483e+09	1.307e+09	0.000e+00	1.028e+09	4.955e-03
913	975	944	8.642e+08	8.440e+08	0.000e+00	7.156e+08	4.422e-03
975	987	981	6.056e+09	3.671e+09	0.000e+00	4.482e+09	3.950e-03
987	1027	1007	5.569e+09	4.984e+09	0.000e+00	4.419e+09	5.021e-03

This article is protected by copyright. All rights reserved.

Author Manuscript

1027	1050	1038.5	6.309e+09	5.796e+09	0.000e+00	4.235e+09	4.825e-03

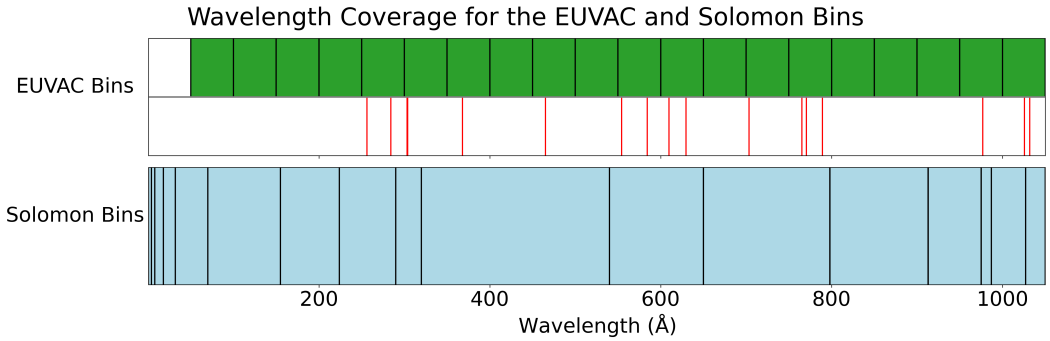


Figure 1: Wavelength coverage for the b37 bins (top) and the b22 bins (bottom). The green region corresponds to the EUVAC bins that are divided into wavelength ranges of variable with. The red vertical lines denote the specific EUV emission lines in the EUVAC binning scheme. The light blue region shows the b22 bins divided into wavelength ranges of variable width. There are no distinct emission lines that are part of the b22 bins.

Figure 2 shows an example of the data (excluding NEUVAC outputs) in the b37 bins and in the b22 bins in three different wavelengths throughout the EUV spectral range. The data are displayed as a function of $P = \frac{1}{2}(F_{10.7} + F_{10.7A})$. It is immediately apparent that EUVAC and HEUVAC are for all intents and purposes, indistinguishable, and are limited in their ability to describe the variability of EUV irradiance in comparison to FISM2. Additionally, HFG and EUVAC-22 both overestimate FISM2. HFG has significant variance compared to other models, and it tends to worsen in its overestimation of FISM2 at high solar activity. The high variance of HFG in comparison to EUVAC-22 is significant enough that a mere 1% increase in F10.7 translates to percent increases in irradiance beyond 3% in multiple wavelength bins, compared to corresponding increases no greater than 1.5% for EUVAC-22.

Note also that HEUVAC and EUVAC are linear with P, so they are straight lines, while FISM2 has significant spread. HFG is not linearly-dependent on P (despite linearity in F10.7 and F10.7A), so it also has spread when comparing to P.

We discuss the specifics of our wavelength rebinning scheme, in which we handle wavelength ranges and specific wavelength emission lines separately, in Appendix A.

2.2 Nonlinear Model Parameterization

A nonlinear parameterization is employed for the model of irradiance across the b59 bins (which include the b37 bins) and the b22 bins, with F10.7 and F10.7B as the inputs. NEUVAC uses a nonlinear parameterization in order to ensure that the distribution of FISM2 irradiances in each bin is better captured by the model. NEUVAC limits itself to 6 model parameters per bin in order to avoid overfitting. The NEUVAC irradiance $\Phi_{N,i}(t)$ at time t in a given wavelength band i, is defined as:

$$\Phi_i(t) = A_i \left[F_{10.7}^{B_i}(t)\right] + C_i \left[F_{10.7B}^{D_i}(t)\right] + E_i \left[F_{10.7B}(t) - F_{10.7}(t)\right] + F_i, \tag{4}$$

This article is protected by copyright. All rights reserved.

Author Manuscript

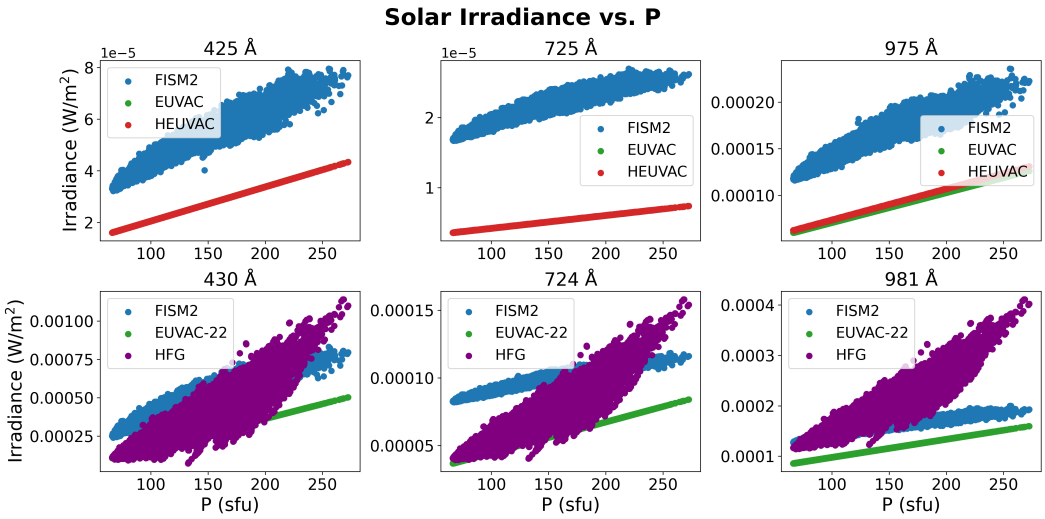


Figure 2: EUV irradiance in 3 wavelength bands in the b37 bins (top) and the 3 nearest corresponding wavelengths in the Solomon bins (bottom). FISM2 data are in blue, EUVAC-37/22 data are in green, HEUVAC-37 data are in red, and HFG data are in purple.

where $A_i, ...F_i$ are parameters determined via linear regression, and $F_{10.7}(t)$ and $F_{10.7B}(t)$ represent F10.7 and F10.7B at time t. NEUVAC was formulated using FISM2 daily irradiances extending back to 1951, provided by the LASP Interactive Solar Irradiance Datacenter (LASP, 2005). We used F10.7 and F10.7B values corrected to 1 AU (Tapping, 2013), with flares removed. These were obtained via the Collect Localisation Satellites (CLS) group in France (`https://spaceweather.cls.fr/services/radioflux/`). We use the 54-day trailing mean of F10.7 in order to take into account 2 preceding solar rotations, during which modulations of the large-scale coronal magnetic field take place, and slowly-varying photospheric features can persist (Poland, 1978; Zherebtsov et al., 1997; Rouillard et al., 2010).

An example of the results of fitting the nonlinear model in both the b37 bins and the b22 bins can be found in Figure 3 (at the same wavelengths as Figure 2). We observe that the NEUVAC model is able to reproduce very well the average behavior of FISM2, without sacrificing the variability in irradiance that is often lost when using a linear model.

2.3 Uncertainty Quantification

We perform uncertainty quantification (UQ) through assessment of the residuals of historical NEUVAC estimates over which the base model was fit, in conjunction with the statistical properties of those same residuals. We employ Monte Carlo (MC) methods to obtain the probability distributions for NEUVAC irradiances in each wavelength bin. These distributions are determined from residuals between the initial NEUVAC fit and FISM2 in each bin, and since the residuals in each bin are correlated, we take into account their covariance. This approach is essentially the standard forward UQ approach but under the condition that the input random variables (F10.7 and F10.7B) are drawn from a probability distribution that is taken to be known with complete certainty (Sullivan, 2015; Zhang, 2021). The result of this procedure is that by repeatedly running NEUVAC, an ensemble of irradiance estimates is generated, from which a confidence interval can

This article is protected by copyright. All rights reserved.

Author Manuscript

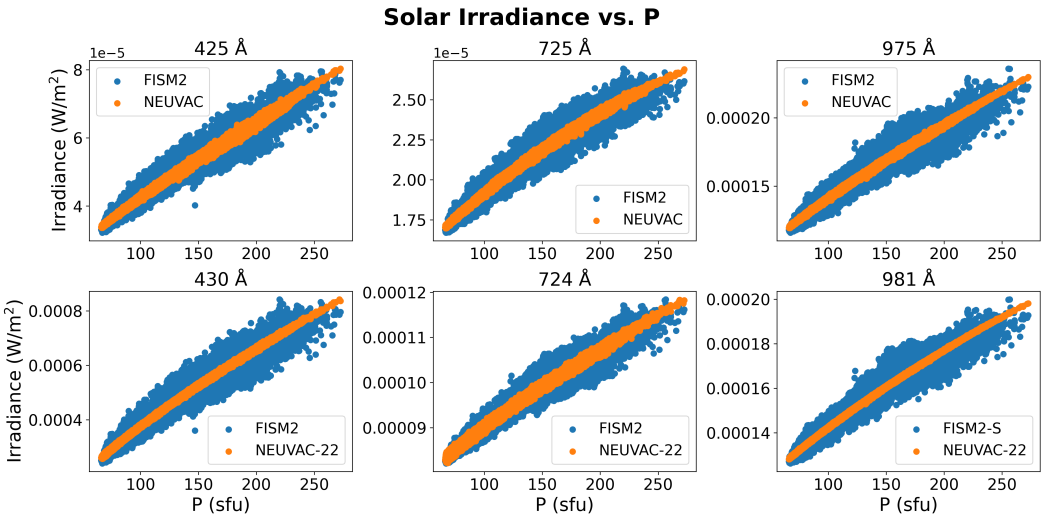


Figure 3: EUV irradiance in 3 wavelength bands in the b37 bins (top) and the 3 nearest corresponding wavelengths in the b22 bins (bottom). FISM2 data are in blue and NEUVAC-37/22 results are in orange.

be determined to describe the region which the true values of irradiance may be found. This ensemble approach has been used for UQ in other contexts such as solar flare forecasting (Guerra et al., 2015), simulations of the ring current (M. W. Chen et al., 2018), and F10.7 forecasting (Daniell & Mehta, 2024).

We note that there are other techniques that could be applied for UQ for NEUVAC. For example, one may find the error distributions in each bin, and then randomly sample from that distribution each time NEUVAC is run for a given F10.7, F10.7B pair. This approach is advantageous due to its simplicity and ability to capture the statistical behavior of a system when there are a large number of measurements for which to calculate the distributions. We however avoided using this method since it assumes that irradiance in each bin can be treated as independent and identical distributed random variables; it takes no account of the fact that the irradiance in different bins are mutually correlated. Another approach involves computing the residuals in each bin, and determining how and if they vary as a function of the value of the irradiance in the bin itself. This approach, however, is even more naive than the one previously-mentioned, and in assuming a functional relationship between irradiance and error, does not faithfully preserve in the estimated irradiance the statistical characteristics of the true irradiance.

Instead of pursuing the aforementioned simpler UQ methods, we implement the specific version of our MC forward UQ approach as follows:

1. The fitting of the base NEUVAC model coefficients is performed between F10.7, F10.7B and rebinned FISM2 irradiances $\Phi_{FISM2,i}$ between 1951 and 2023, using Equation 4.
2. Historical NEUVAC irradiances $\Phi_{N,i}$ are generated for that time period.
3. Residuals Δ_i between $\Phi_{FISM2,i}$ and $\Phi_{N,i}$ are computed over the time period for fitting.
4. The normalized covariance matrix $\tilde{\mathbf{C}}$ is computed from Δ_{ij}, where C_{ij} denotes the cross-correlation between Δ_i and Δ_j.

This article is protected by copyright. All rights reserved.

Author Manuscript

5. The normalized standard deviation $\sigma_{N,i}$ in each band i is computed from Δ_i, where for a single band:

$$\sigma_{N,i} = \frac{\text{STD}\left(\Phi_{FISM2,i} - \Phi_{N,i}\right)}{\Phi_{N,i}} \tag{5}$$

where 'STD' refers to the standard deviation.

This is done because the brightness in the different EUV bins are highly correlated with each other. This means that if an ensemble of irradiances is created using given values of F10.7 and F10.7B, the spectra need to include this correlation. In order to create an ensemble member, the following procedure (applied to each wavelength band) is used:

1. A random number P_i is drawn from a normal distribution with mean 0 and standard deviation of 1. The first obtained P_i value is denoted $P_{i,0}$, and used in all following computations of the normalized correlated perturbation (for all later irradiance ensemble members).
2. The normalized correlated perturbation N_i is computed as $N_i = C_{i,k}P_{i,0}+(1 - C_{i,k})\,P_i$. Note that $C_{i,k}$ is obtained from $\tilde{\mathbf{C}}$: When NEUVAC is run in the b59 bins, it is the normalized correlation of band i with the first wavelength band ($k = 0$) of the b59 bins (equivalently the first wavelength band of the b37 bins) when $i < 7$ and the eighth wavelength band ($k = 7$) when $i \geq 7$, and when NEUVAC is run in the b22 bins, it is the normalized correlation of band i is with the first wavelength band ($k = 0$) of the b22 bins when $i < 5$ and the sixth wavelength band when $i \geq 5$. We stress that the choice of k affects the spread of the ensemble and was chosen so that perturbations in each band move by an amount that incorporates their correlation with another wavelength bin. A poor choice of k corresponds to a wavelength bin with which nearly all others in some range are weakly correlated, whereas a good choice of k corresponds to the reverse. We chose two values of k in two ranges since the EUV bins near the soft x-ray range behave differently than those outside of it.
3. Scaling with the standard deviation is performed to yield $A_i = \sigma_{N,i}N_i$.
4. The irradiance ensemble member is obtained via $\Phi_{N,i} * (1 - A_i)$

The resulting ensemble of irradiances form a distribution which may be used for uncertainty quantification. In all results below, we show results of the ensemble mean of 100 NEUVAC ensemble runs ($\Phi_{E,i}$). We show the covariance matrix $\tilde{\mathbf{C}}$ for the b59 bins and the b22 bins in Figure 4. We implement the entirety of NEUVAC and the associated UQ in Python relying primarily on the NumPy (Harris et al., 2020) and Seaborn (Waskom, 2021) packages.

2.4 Validation

For validation, we compare model results to FISM2 outputs in the relevant bins, and use the percentage deviation δ, defined below:

$$\delta_i(t) = \frac{\Phi_{M,i}(t) - \Phi_{FISM2,i}(t)}{\Phi_{FISM2,i}(t)} \times 100\% \tag{6}$$

as well the mean absolute percentage error (MAPE), defined as follows:

$$MAPE = \frac{1}{n}\sum_{t=1}^{n}\left|\frac{\Phi_{M,i}(t) - \Phi_{FISM2,i}(t)}{\Phi_{FISM2,i}(t)}\right| \tag{7}$$

This article is protected by copyright. All rights reserved.

Author Manuscript

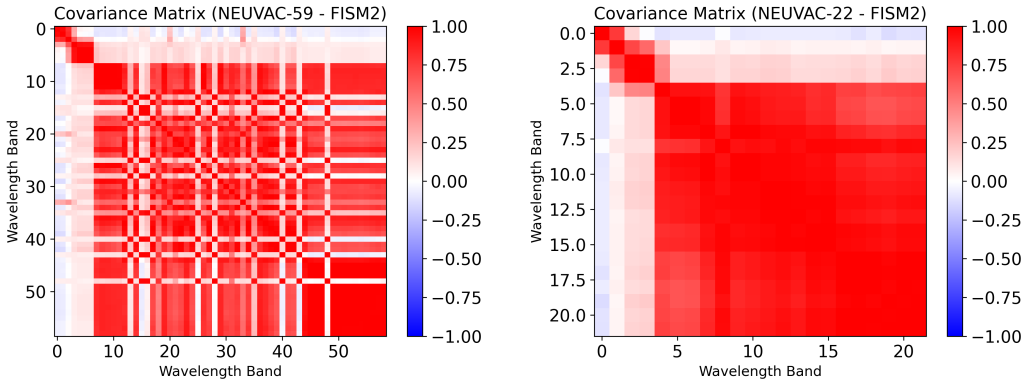


Figure 4: The normalized covariance matrix $\tilde{\mathbf{C}}$ for the b59 bins (left) and the b22 bins (right).

where $\Phi_{FISM2,i}(t)$ is the ith irradiance value from FISM2 at time t, and $\Phi_{M,i}(t)$ is the ith irradiance value either modeled by NEUVAC, EUVAC, HEUVAC or HFG.

Figure 5 shows the distribution of δ between NEUVAC-59 and FISM2, and NEUVAC-22 and FISM2, in 6 different wavelength bands, corresponding to the entire period of time used to perform the fitting. Kernel Density Estimation (Rosenblatt, 1956; Parzen, 1962) was used to generate the approximate probability density for each distribution. Each distribution is centered around zero, showing the overall accuracy of NEUVAC. We note that at the lower wavelengths, (namely 425 Å and 430 Å), the spread of the distribution is wider, with maximum deviations approaching ±20%. This highlights the difficulty of modeling irradiance at wavelengths approaching those of soft x-rays, which are significantly enhanced in response to solar active regions (Briand et al., 2021).

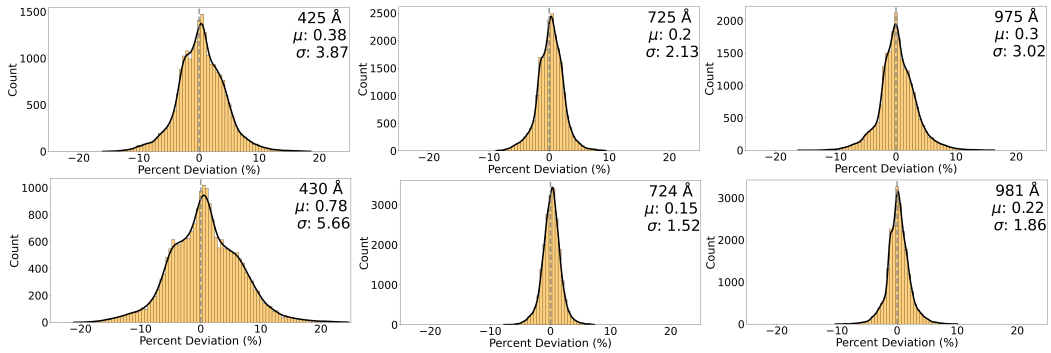


Figure 5: Distributions of percent deviation between NEUVAC and FISM for NEUVAC-59 (top row) and NEUVAC-22 (bottom row) at the same wavelengths as considered in Figure 3. The histograms show the number (count) of values in each bin, and in each plot, μ is the arithmetic mean, and σ is the standard deviation of the distribution.

These results indicate similar performance of NEUVAC in both the b59 and b22 bins. While there are minor discrepancies in the distributions of δ in both bins for the wavelengths shown in Figure 5, the wavelength bins of b22 are in many cases significantly larger than that of b59. As such, the variability of irradiance within those bins is dom-

This article is protected by copyright. All rights reserved.

Author Manuscript

inated by the variable bright solar lines they contain, thereby affecting the error distributions for NEUVAC-59 in comparison to NEUVAC-22, even when the center wavelength of the bins is very close.

3 Results

We first show sample spectra (excluding bright emission lines) for all of the models during low solar activity (March 30, 2004) and high solar activity (February 2, 2002), respectively (Figure 6). In the b37 bins, the ensemble average of 100 NEUVAC runs is almost indistinguishable from FISM2. Additionally, EUVAC and HEUVAC exhibit no significant differences, except in the vicinity 350 Å, where EUVAC is lower than HEUVAC during solar minimum. EUVAC and HEUVAC generally overestimate FISM2 below 350 Å and underestimate FISM2 above 350 Å during low and high solar activity, respectively.

In the b22 bins, there are noticeable differences between the behavior of EUVAC-22 and HFG. During solar minimum, below 300 Å, EUVAC-22 overestimates FISM2 while HFG underestimates FISM2. In contrast, between 300 Å and 600 Å, HFG matches FISM2 more closely than EUVAC. During solar maximum, EUVAC-22 generally overestimates FISM2 below 400 Å and underestimates it above 400 Å. In comparison HFG underestimates FISM2 more often below 600 Å, and overestimates it above 600 Å. These results confirm those initially reported by Solomon and Qian (2005) (c.f. Figure 1 of the same), though we note that there may be discrepancies owing to the fact that in this paper, the irradiance in overlapping bins was simply summed together before being displayed.

3.1 MAPE Analysis

We next consider the values of the Mean Absolute Percentage Error as a function of wavelength band for both the b37 bins and the b22 bins, across the entire dataset spanning years between 1963 and 2023 inclusive (Figure 7). EUVAC and HEUVAC display overall performance closest to NEUVAC at wavelengths below 300 Å. NEUVAC, by comparison demonstrates increasingly accurate performance as wavelength increases, with values of MAPE that are lowest between 600 and 800 Å. EUVAC and HEUVAC, by comparison, show values of MAPE that oscillate nearly symmetrically around 50% for wavelengths greater than 300 Å.

Results in the b22 bins show a similar difference of behavior between NEUVAC-22 and EUVAC-22 and HFG, save that values of MAPE for EUVAC-22 are much closer to that of NEUVAC-22 above 900 Å. As is seen in the b37 bins, values of MAPE for NEUVAC-22 slightly increase as a wavelength increases, while for EUVAC-22, they slightly decrease as wavelength increases. The greatest values of MAPE for EUVAC-22 and HFG occur below 50 Å. In contrast to the b37 bins, values for EUVAC-22 and HFG remain approximately 60%, lower than the higher values the non-NEUVAC models attained in the b37 bins. This behavior is shared by NEUVAC-22, which attained values on the order of 7%, compared to $\sim$5% for NEUVAC-37.

Figure 8 shows percent deviations with respect to FISM2, in select wavelength bands as a function of F10.7. The spread of NEUVAC percent deviation values remains clustered about zero in each case, indicating that even at extreme levels of solar activity (during which variability in EUV is most intense due to the prominence of highly-transient active regions), NEUVAC maintains appreciable accuracy. In contrast, percent deviations are clustered around negative values for EUVAC and HEUVAC in the b37 bins, indicating that EUVAC and HEUVAC underestimate FISM2 at these wavelengths, though the slightly positive trend in the percent deviation suggests that H/EUVAC has a slight bias towards higher solar activity.

This article is protected by copyright. All rights reserved.

Author Manuscript

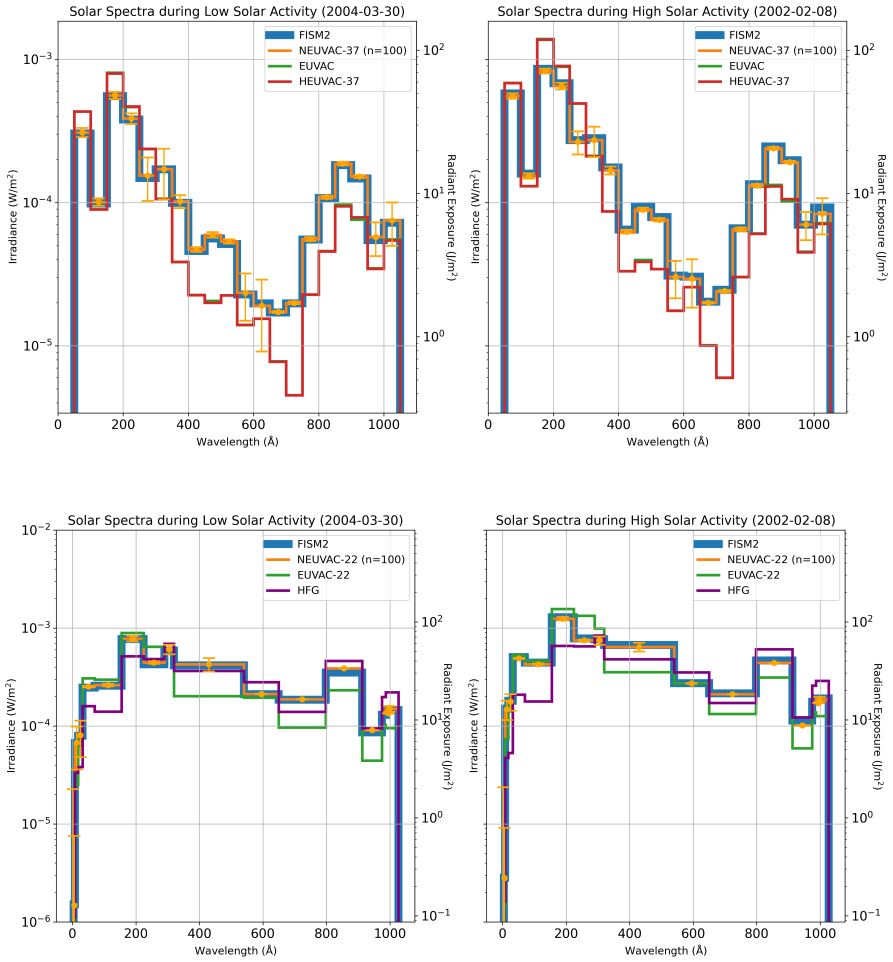


Figure 6: Top: Solar spectra in the b37 bins during low (left) and high (right) solar activity. Bottom: Same as the top but for the b22 bins.

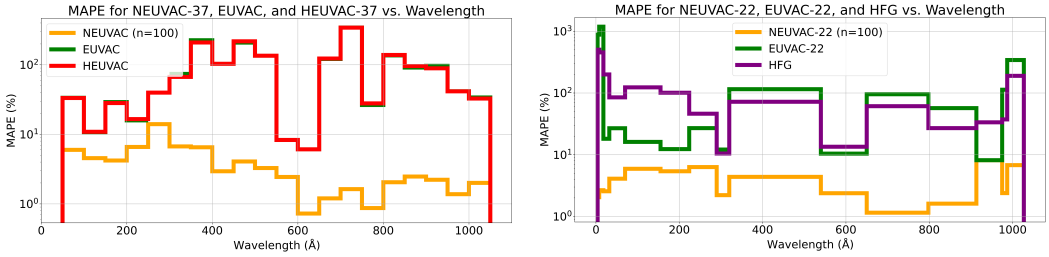


Figure 7: Values of MAPE as a function of wavelength band for NEUVAC, EUVAC, and HEUVAC (left) and for NEUVAC-22, EUVAC-22, and HFG (right).

In the b22 bins, the percent deviations for EUVAC-22 and HFG have biases that are increasing with increasing solar activity compared to NEUVAC, with those corresponding to HFG being the most strongly positive. This indicates that, in a number of bands, EUVAC-22 and HFG have the lowest accuracy at high levels of solar activity. The general trend of systemic underestimation by EUVAC-22 comports well with the fact that the F74113 spectrum on which it is based was obtained via rocket measurement on April

This article is protected by copyright. All rights reserved.

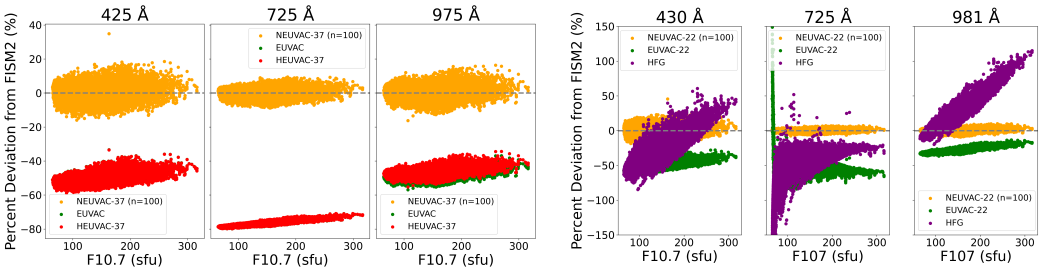


Figure 8: Percent deviations from FISM2 as a function of F10.7: at 425, 725, and 975 Å in the EUVAC bins (left) and at 430, 724, and 981 Å in the Solomon bins (right).

23, 1974, which was well into the declining phase of Solar Cycle 20, and highlights again the known issue of consistent underestimation by HFG originally observed by P. Richards and Torr (1984).

Table 3 shows how the MAPE values for all models vary as a function of solar activity. In the calculation of these values, we considered the energy integrated across all bins, for both the b37 bins and the b22 bins. We follow Jin et al. (2021) in denoting low solar activity as F10.7 $<$ 80 sfu, moderate solar activity as 80 sfu $\leq$ F10.7 $<$ 120 sfu, and high solar activity as F10.7 $\geq$ 120 sfu. We observe, consistent with previous observations, that NEUVAC MAPE values are lowest in both the b37 and the b22 bins.

Interestingly, however, NEUVAC MAPE values are proportional to solar activity in EUVAC bins but they are *inversely* proportional to solar activity in the Solomon bins. This behavior is not observed for EUVAC/HEUVAC-37 and EUVAC-22. HFG MAPE values were also inversely proportional to solar activity in the b22 bins. In the b37 bins, MAPE values for HEUVAC-37 were the highest at moderate activity, while they were highest for EUVAC at low and high activity. These results indicate that in the b37 bins, the best performance of H/EUVAC will be at moderate activity, and in the b22 bins, the best performance of EUVAC will be at moderate activity, and that of HFG will be observed at high solar activity.

Model	MAPE (Low Activity)	MAPE (Moderate Activity)	MAPE (High Activity)
NEUVAC-37	3.50	3.41	3.99
EUVAC	9.12	5.75	8.37
HEUVAC-37	8.54	5.87	8.32
NEUVAC-22	13.48	12.57	9.88
EUVAC-22	24.99	20.06	9.65
HFG	41.47	36.59	22.77

Table 3: Values of MAPE as a function of solar activity, for energy integrated across all bins: the sky blue-colored rows correspond to the b37 bins and the salmon-colored rows correspond to the b22 bins.

This article is protected by copyright. All rights reserved.

Author Manuscript

Author Manuscript

3.2 Time Series

We also evaluated time series of irradiance at several wavelength bands in order to evaluate NEUVAC's performance during solar minimum and solar maximum. An example of time series of irradiance during the ascending phase of Solar Cycle 25 is shown for NEUVAC (centered at 425 Å in the b37 bins) and NEUVAC-22 (centered at 430 Å in the b22 bins) in Figure 9. For an ensemble run of $n = 100$, the uncertainty bounds corresponding to the range of ensemble results encompass FISM2 throughout nearly the entire time period. Again, as seen in Figure 6, EUVAC and HEUVAC are essentially indistinguishable. More significantly, at 430 Å, HFG corresponds to FISM2 in magnitude more closely than EUVAC-22, even though its variance increases significantly more than that of EUVAC as solar maximum approaches.

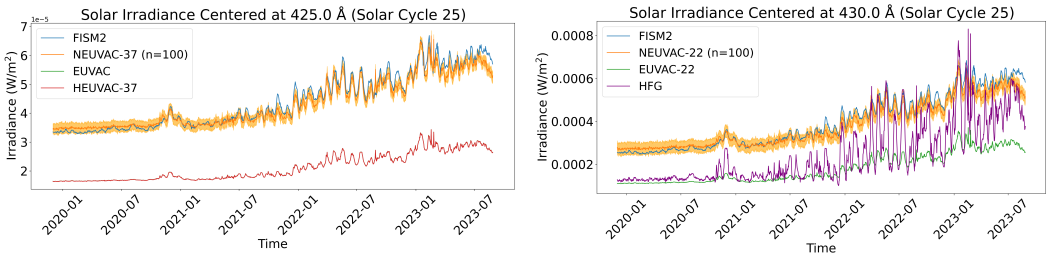


Figure 9: Time series of solar EUV irradiance centered at 425 Å in the b37 bins (left) and at 430 Å in the b22 bins (right), during the entirety of the ascending phase of Solar Cycle 25.

A more comprehensive analysis of time series of solar EUV irradiance in both the EUVAC bins and the Solomon bins is shown Figure 10, where the first and third rows correspond to solar minimum (end of Solar Cycle 21) and the second and fourth rows correspond to solar maximum during Solar Cycle 22. The same wavelengths are shown as those in Figures 2 and 3.

In the b37 bins, there is strong correspondence between the ensemble average of NEUVAC and FISM2, along with a consistent underestimation of the magnitude of the irradiance by EUVAC and HEUVAC at all of the considered wavelengths (which are at the low, middle, and high regions of the wavelength ranges of the EUVAC bins). Of note is that the underestimation of energy by EUVAC and HEUVAC grows larger at high solar activity. A small difference between EUVAC and HEUVAC at 975 Å is noted that is not observed at lower wavelengths.

In the b22 bins, the behavior is essentially the same for EUVAC-22. HFG, in comparison shows an increase in accuracy with solar activity, except for irradiance centered at 981 Å. These results call to mind the importance of discrepancies in scaling of the irradiance amplitudes as a function of wavelength, initially pointed out by Lean et al. (2003): while the total energies between the models may be rather close (as will be considered in the following subsection) the absolute scale of the irradiance in any given band may vary significantly between each model. NEUVAC-22 remains close to FISM2 throughout all conditions.

This article is protected by copyright. All rights reserved.

Author Manuscript

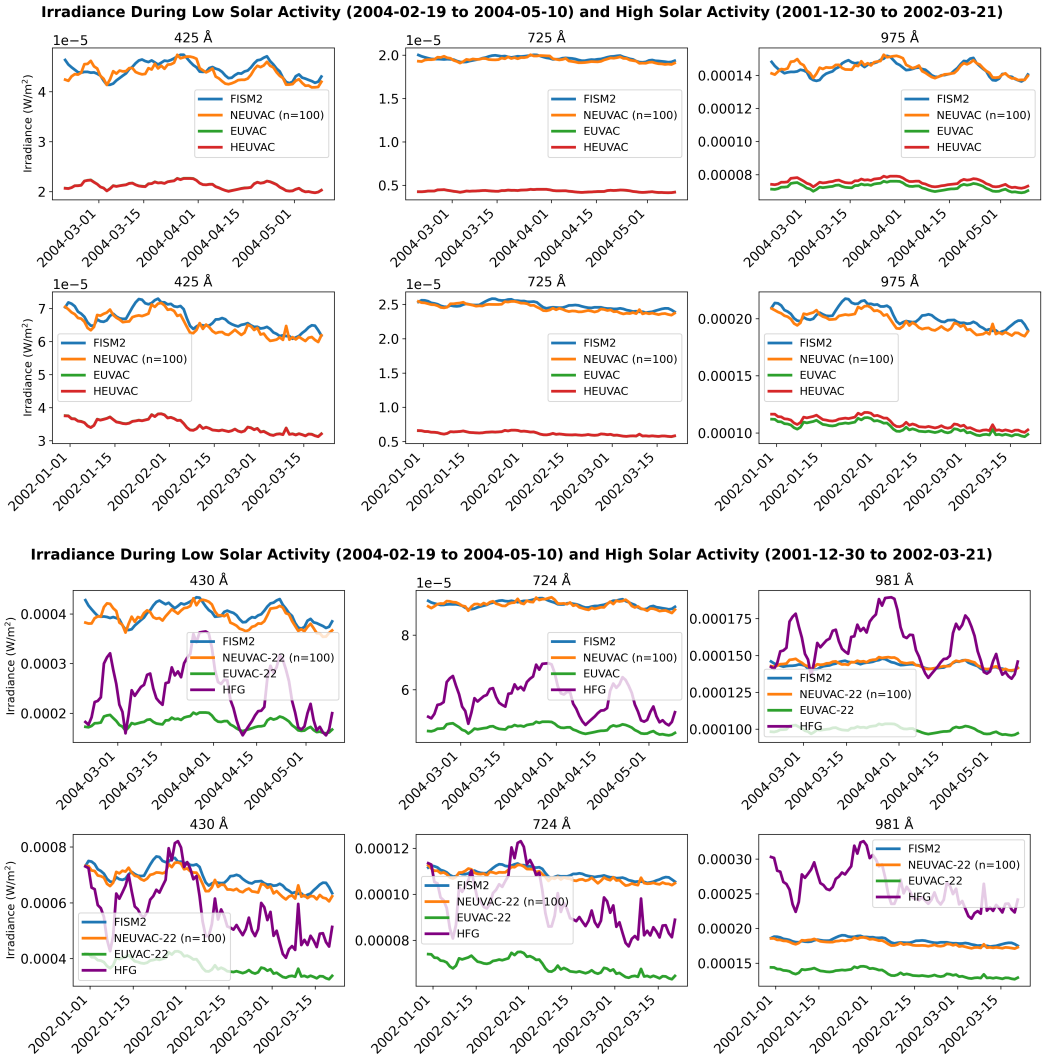


Figure 10: Top: Time series of solar spectra in the b37 bins at 425, 725, and 975 Å (left to right) at solar minimum (top row) and solar maximum (bottom row). Bottom: Time series of solar spectra in the b22 bins at 430, 724, and 981 Å (left to right) at solar minimum (top row) and solar maximum (bottom row).

3.3 Earth-Incident Energy Deposition

Finally, we present an assessment of the total Earth-incident energy estimated by all of the models, in order to broadly survey their quantification of EUV energy applied to the entire solar-terrestrial environment (Figure 11). In the calculation of Earth-incident energy deposition, for each model, we sum the irradiance values across all of the bins, and take the product of that sum with the cross-sectional area of the Earth, where we use the nominal terrestrial radius of the Earth (6.3781×10^6 m) as suggested by Mamajek et al. (2015). The Earth-incident energy presented here corresponds to the EUV incident on the sunward side of the Earth.

NEUVAC tracks FISM2 very well in the b37 bins, during both low and high solar activity, underestimating FISM2 by only $\sim$ 3 GW on in both cases. The EUVAC

This article is protected by copyright. All rights reserved.

Author Manuscript

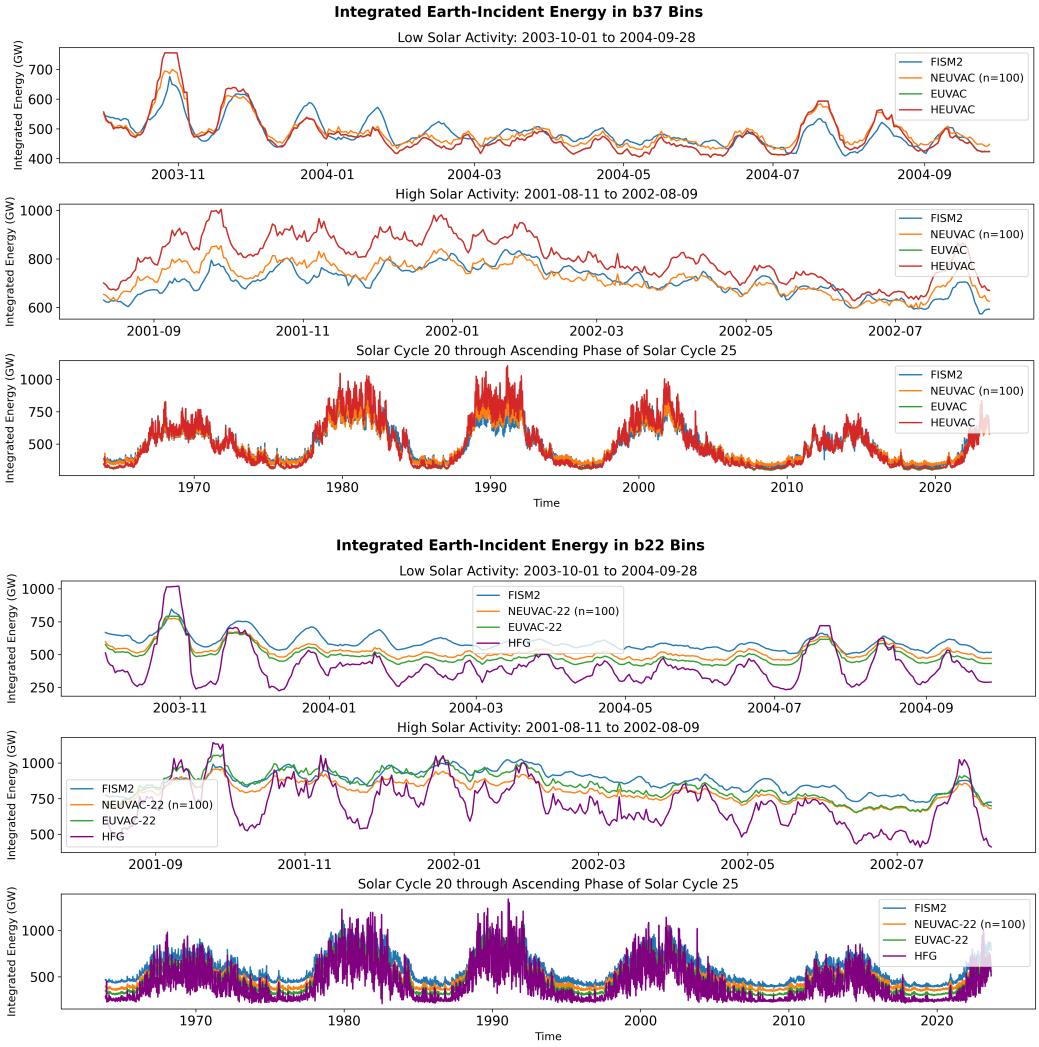


Figure 11: Top: Total integrated EUV energy in GW across all b37 bins at solar minimum (top), solar maximum (middle), and throughout the entire time period considered. Bottom: The Same but in the b22 bins.

and HEUVAC models, by comparison, most strongly track FISM2 at low solar activity with an underestimation of ∼32 GW, but strongly overestimate the total energy during solar maximum, by ∼48 GW on average. The amount of total energy deposited over the time period was very close between all models: NEUVAC differed from FISM2 by $\sim 0.5\%$, while differences were approximately -1.4% and approximately -1.3% for EUVAC and HEUVAC, respectively.

In the b22 bins, NEUVAC underestimates the irradiance in comparison to FISM2, most severely during solar maximum (by an average of ~ 76 GW), as compared to solar minimum (where the underestimation is on average ~ 59 GW). The EUVAC model also underestimated irradiance compared to FISM2, by $\sim$ 108 GW during solar minimum and by ~ 64 GW during solar maximum. The HFG model in particular is strongly variable, especially at high solar activity, underestimating irradiance the most compared to the rest of the models. During solar minimum, HFG's estimation was most severe (by ~ 180 GW) compared to solar maximum (by ~ 163 GW). Regarding total energy de-

This article is protected by copyright. All rights reserved.

Author Manuscript

posited over the time period, NEUVAC-22 differed from FISM2 by $\sim 11.72\%$, while differences were $\sim 17.07\%$ and $\sim 32.14\%$ for EUVAC-22 and HFG, respectively.

We wish to emphasize that overall, the b22 bins don't allow modeling the total energy input into the thermosphere-ionosphere as accurately the b37 bins. This can be seen in the much larger percent errors in the models for total energy in the b22 bins compared to the b37 bins.

4 Summary

A Nonlinear Extreme Ultraviolet Irradiance Model for Aeronomic Calculations (NEUVAC) has been developed, based on nonlinear fits between F10.7, F10.7B and solar irradiance estimated by the FISM2 model. The model has been developed in 59 wavelengths bins used by the GITM model, as well as in the Standard Bands initially presented by Solomon and Qian (2005), in order to support immediate ingestion into global ionosphere-thermosphere models. The model approximates the FISM2 irradiances to a high degree of accuracy, and is capable of running ensembles for uncertainty quantification. As shown by MAPE values, the model performs with $< 5\%$ error under all solar conditions in the EUVAC bins, and with $< 15\%$ error under all solar conditions in the Solomon bins. The model represents an innovation in that it reproduces the FISM2 flux with high accuracy from an index that is nearly always obtainable without gaps, and may be predicted with a variety of methods (Huang et al., 2009; Henney et al., 2012; Warren et al., 2017; Du, 2020; Petrova et al., 2021; Stevenson et al., 2022; Daniell & Mehta, 2023; Hao et al., 2024). To this end, we recommend NEUVAC for consideration in the context of operational space weather nowcasting and forecasting.

Future work will involve the running of GITM with NEUVAC irradiance ensembles to perform uncertainty quantification on downstream ionosphere-thermosphere parameters both directly and indirectly connected to solar EUV irradiance. Additional development of the NEUVAC model will include extending the uncertainty quantification component inherent in its running of ensembles by parameterizing ensemble generation in terms of correlations of residuals between *all* bins, instead of just two bins. NEUVAC will also be investigated in terms of its effects on altitude-dependent photoionization and photodissociation rates, given the importance of these rates in affecting ionosphere-thermosphere composition. Long-term, comprehensive development of a successor model will be undertaken, in order to assess the strengths of the nonlinear paradigm in modeling EUV irradiance in terms of a single proxy. This model development will take advantage of historical EUV measurements as well as those which may be taken by a number of future missions (Young, 2021).

5 Open Research

NEUVAC was developed with Sun-Earth distance adjusted and flare-corrected F10.7 values provided by Collecte Localisation Satellites (Collecte Localisation Satellites, 2000). FISM2 data were obtained via LISIRD, which is curated by the University of Colorado, Boulder (LASP, 2005). NEUVAC is available via GitHub repository as part of the EUVpy irradiance package, and available also via Zenodo (Brandt & Ridley, 2024).

Appendix A Wavelength Rebinning

The native FISM2 data require rebinning into the b59 bins. However, there is a complication in that some of the "bins" are single wavelength lines, while others are bins that are wider than the FISM2 bins. These therefore must be treated separately.

For the b59 and b37 bins that are wider than the FISM2 bins, the calculation works by summing the irradiances multiplied by the FISM2 bin width ($\delta\lambda$=0.1 nm):

This article is protected by copyright. All rights reserved.

Author Manuscript

$$\Phi^i_{bin} = \sum_{low^i}^{high^i} \Phi_{FISM2}\delta\lambda \tag{A1}$$

where Φ^i_{bin} is one of the wider EUV bins, low^i and $high^i$ represent the low and high wavelengths of the bin i, where the low bin is included and the high bin is excluded. Φ_{FISM2} is the irradiance from FISM2.

For the individual spectral lines, the irradiance in a 4-nm centered window around the FISM2 emission line is summed, multiplied by the FISM2 bin width, and then assigned to the GITM bin:

$$\Phi^i_{bin} = \sum_{\lambda-20\delta\lambda}^{\lambda+20\delta\lambda} \Phi_{FISM2}\delta\lambda \tag{A2}$$

There are two complicating factors with this method:

1. Due to the fact that these individual lines are in the middle of normal b59 and b37 bins, it is unclear if the irradiance should be zeroed out before calculating the irradiances in the larger bins.
2. There are sometimes lines that end up being in the same FISM2 bin. It is unclear whether the irradiance intensity within the FISM2 bin should be divided between the two lines in some way.

For the present study, we have elected to zero out the irradiance in the individual lines before determining the binned irradiances in the remaining wavelength ranges.

Acknowledgments

The authors are grateful for valuable insight regarding statistics needed to develop NEUVAC from Michigan Tech Research Institute personnel, including Dr. Brian Thelen, Dr. Sarah Kitchen, and Mr. Brian Wilson. We are also grateful for insights into the workings of HEUVAC provided by Dr. Phil G. Richards, Dr. Jeongeon Kim, and Dr. Matthew Kehoe, and for the curation of LISIRD by staff at CU Boulder. Development of NEUVAC and the EUVpy package of which it is a part was partially supported by NASA Grant #80NSSC20K1581.

References

Akmaev, R. A., Fuller-Rowell, T., Wu, F., Forbes, J., Zhang, X., Anghel, A., ... Juang, H.-M. (2008). Tidal variability in the lower thermosphere: Comparison of whole atmosphere model (wam) simulations with observations from timed. *Geophysical Research Letters*, *35*(3).

Anderson, P. C., & Hawkins, J. M. (2016). Topside ionospheric response to solar euv variability. *Journal of Geophysical Research: Space Physics*, *121*(2), 1518–1529.

Bertello, L., Ulrich, R. K., & Boyden, J. E. (2010). The mount wilson ca ii k plage index time series. *Solar Physics*, *264*, 31–44.

Bilitza, D., Pezzopane, M., Truhlik, V., Altadill, D., Reinisch, B. W., & Pignalberi, A. (2022). The international reference ionosphere model: A review and description of an ionospheric benchmark. *Reviews of Geophysics*, *60*(4), e2022RG000792.

This article is protected by copyright. All rights reserved.

Author Manuscript

Brandt, D. A., & Ridley, A. J. (2024). *Euvpy [software].* Retrieved from `https://github.com/DanBrandt/EUVpy` (Version 1.0-prealpha) doi: 10.5281/zenodo.13685579

Brandt, D. A., Vega, E. F., & Ridley, A. J. (2024). On generalized additive models for representation of solar euv irradiance. *Space Weather*, *22*(3), e2023SW003680.

Briand, C., Doerksen, K., & Deleflie, F. (2021). Solar euv-enhancement and thermospheric disturbances. *Space Weather*, *19*(12), e2021SW002840.

Brueckner, G., Edlow, K., Floyd IV, L., Lean, J., & VanHoosier, M. (1993). The solar ultraviolet spectral irradiance monitor (susim) experiment on board the upper atmosphere research satellite (uars). *Journal of Geophysical Research: Atmospheres*, *98*(D6), 10695–10711.

Bussy-Virat, C. D., Ridley, A. J., & Getchius, J. W. (2018). Effects of uncertainties in the atmospheric density on the probability of collision between space objects. *Space Weather*, *16*(5), 519–537.

Chamberlin, P. C., Eparvier, F. G., Knoer, V., Leise, H., Pankratz, A., Snow, M., ... Woods, T. N. (2020). The flare irradiance spectral model-version 2 (fism2). *Space Weather*, *18*(12), e2020SW002588.

Chamberlin, P. C., Woods, T. N., & Eparvier, F. G. (2007). Flare irradiance spectral model (fism): Daily component algorithms and results. *Space Weather*, *5*(7).

Chamberlin, P. C., Woods, T. N., & Eparvier, F. G. (2008). Flare irradiance spectral model (fism): Flare component algorithms and results. *Space Weather*, *6*(5).

Chen, M. W., O'Brien, T. P., Lemon, C. L., & Guild, T. B. (2018). Effects of uncertainties in electric field boundary conditions for ring current simulations. *Journal of Geophysical Research: Space Physics*, *123*(1), 638–652.

Chen, Y., Liu, L., & Wan, W. (2011). Does the f10. 7 index correctly describe solar euv flux during the deep solar minimum of 2007–2009? *Journal of Geophysical Research: Space Physics*, *116*(A4).

Clette, F., & Lefèvre, L. (2016). The new sunspot number: assembling all corrections. *Solar Physics*, *291*, 2629–2651.

Codrescu, M. V., Negrea, C., Fedrizzi, M., Fuller-Rowell, T., Dobin, A., Jakowsky, N., ... Maruyama, N. (2012). A real-time run of the coupled thermosphere ionosphere plasmasphere electrodynamics (ctipe) model. *Space Weather*, *10*(2).

Collecte Localisation Satellites. (2000). *Solar flux archive [dataset].* Retrieved 2024-08-30, from `ftp://ftpsedr.cls.fr/pub/previsol/solarflux/observation/radio_flux_adjusted_observation.txt`

Daniell, J. D., & Mehta, P. M. (2023). Probabilistic solar proxy forecasting with neural network ensembles. *Space Weather*, *21*(9), e2023SW003675. Retrieved from `https://agupubs.onlinelibrary.wiley.com/doi/abs/10.1029/2023SW003675` (e2023SW003675 2023SW003675) doi: https://doi.org/10.1029/2023SW003675

Daniell, J. D., & Mehta, P. M. (2024). Probabilistic short-term solar driver forecasting with neural network ensembles. *Space Weather*, *22*(3), e2023SW003785.

de Wit, T. D., Kretzschmar, M., Aboudarham, J., Amblard, P.-O., Auchère, F., & Lilensten, J. (2008). Which solar euv indices are best for reconstructing the solar euv irradiance? *Advances in Space Research*, *42*(5), 903–911.

Du, Z. (2020). Forecasting the daily 10.7 cm solar radio flux using an autoregressive model. *Solar Physics*, *295*(9), 125.

Dudok de Wit, T., Kretzschmar, M., Lilensten, J., & Woods, T. (2009). Finding the best proxies for the solar uv irradiance. *Geophysical Research Letters*, *36*(10).

Elvidge, S., Themens, D. R., Brown, M. K., & Donegan-Lawley, E. (2023). What to do when the f10. 7 goes out? *Space Weather*, *21*(4), e2022SW003392.

This article is protected by copyright. All rights reserved.

Author Manuscript

Girazian, Z., & Withers, P. (2015). An empirical model of the extreme ultraviolet solar spectrum as a function of f10.7. *Journal of Geophysical Research: Space Physics*, *120*(8), 6779–6794.

Guerra, J. A., Pulkkinen, A., & Uritsky, V. M. (2015). Ensemble forecasting of major solar flares: First results. *Space Weather*, *13*(10), 626–642.

Hao, Y., Lu, J., Peng, G., Wang, M., Li, J., & Wei, G. (2024). F10. 7 daily forecast using lstm combined with vmd method. *Space Weather*, *22*(1), e2023SW003552.

Harris, C. R., Millman, K. J., van der Walt, S. J., Gommers, R., Virtanen, P., Cournapeau, D., ... Oliphant, T. E. (2020, September). Array programming with NumPy. *Nature*, *585*(7825), 357–362. Retrieved from `https://doi.org/10.1038/s41586-020-2649-2` doi: 10.1038/s41586-020-2649-2

Hedin, A., & Mayr, H. (1987). Solar euv induced variations in the thermosphere. *Journal of Geophysical Research: Atmospheres*, *92*(D1), 869–875.

Henney, C., Hock, R., Schooley, A., Toussaint, W., White, S., & Arge, C. (2015). Forecasting solar extreme and far ultraviolet irradiance. *Space Weather*, *13*(3), 141–153.

Henney, C., Toussaint, W., White, S., & Arge, C. (2012). Forecasting f10. 7 with solar magnetic flux transport modeling. *Space Weather*, *10*(2).

Heroux, L., & Hinteregger, H. (1978). Aeronomical reference spectrum for solar uv below 2000 å. *Journal of Geophysical Research: Space Physics*, *83*(A11), 5305–5308.

Hinteregger, H. (1981). Representations of solar euv fluxes for aeronomical applications. *Advances in Space Research*, *1*(12), 39–52.

Hinteregger, H., Bedo, D., Manson, J., & Skillman, D. (1976). Euv flux variations with solar rotation observed during 1974-1976 from ae satellites c, d, and e. In *Cospar meeting.*

Hinteregger, H. E., Fukui, K., & Gilson, B. R. (1981). Observational, reference and model data on solar euv, from measurements on ae-e. *Geophysical Research Letters*, *8*(11), 1147–1150.

Huang, C., Liu, D.-D., & Wang, J.-S. (2009). Forecast daily indices of solar activity, f10. 7, using support vector regression method. *Research in Astronomy and Astrophysics*, *9*(6), 694.

Jin, H., Zou, S., Yan, C., Yang, G., Chen, G., Zhang, S., ... Wang, Z. (2021). A statistical study of f-region 3.2-m-scale field-aligned irregularities occurrence and vertical plasma drift over hainan: Solar activity, season, and magnetic activity dependences. *Journal of Geophysical Research: Space Physics*, *126*(5), e2020JA028932.

LASP. (2005). *"lasp interactive solar irradiance datacenter" [data set].* Laboratory for Atmospheric and Space Physics. Retrieved from `https://lasp.colorado.edu/lisird/` doi: 10.25980/L27Z-XD34

Lean, J., Warren, H., Mariska, J., & Bishop, J. (2003). A new model of solar euv irradiance variability 2. comparisons with empirical models and observations and implications for space weather. *Journal of Geophysical Research: Space Physics*, *108*(A2).

Liu, H.-L., Bardeen, C. G., Foster, B. T., Lauritzen, P., Liu, J., Lu, G., ... others (2018). Development and validation of the whole atmosphere community climate model with thermosphere and ionosphere extension (waccm-x 2.0). *Journal of Advances in Modeling Earth Systems*, *10*(2), 381–402.

Machol, J., Snow, M., Woodraska, D., Woods, T., Viereck, R., & Coddington, O. (2019). An improved lyman-alpha composite. *Earth and Space Science*, *6*(12), 2263–2272.

Mamajek, E., Prsa, A., Torres, G., Harmanec, P., Asplund, M., Bennett, P., ... others (2015). Iau 2015 resolution b3 on recommended nominal conversion constants for selected solar and planetary properties. *arXiv preprint*

This article is protected by copyright. All rights reserved.

Author Manuscript

arXiv:1510.07674.

Maruyama, N., Sun, Y.-Y., Richards, P. G., Middlecoff, J., Fang, T.-W., Fuller-Rowell, T. J., ... Valladares, C. E. (2016). A new source of the midlatitude ionospheric peak density structure revealed by a new ionosphere-plasmasphere model. *Geophysical Research Letters*, *43*(6), 2429–2435.

Parzen, E. (1962). On estimation of a probability density function and mode. *The annals of mathematical statistics*, *33*(3), 1065–1076.

Petrova, E., Podladchikova, T., Veronig, A. M., Lemmens, S., Virgili, B. B., & Flohrer, T. (2021). Medium-term predictions of f10. 7 and f30 cm solar radio flux with the adaptive kalman filter. *The Astrophysical Journal Supplement Series*, *254*(1), 9.

Poland, A. I. (1978). Motions and mass changes of a persistent coronal streamer. *Solar Physics*, *57*, 141–153.

Qian, L., Burns, A. G., Emery, B. A., Foster, B., Lu, G., Maute, A., ... Wang, W. (2014). The ncar tie-gcm: A community model of the coupled thermosphere/ionosphere system. *Modeling the ionosphere–thermosphere system*, 73–83.

Richards, P., Fennelly, J. a., & Torr, D. (1994). Euvac: A solar euv flux model for aeronomic calculations. *Journal of Geophysical Research: Space Physics*, *99*(A5), 8981–8992.

Richards, P., & Torr, D. (1984). An investigation of the consistency of the ionospheric measurements of the photoelectron flux and solar euv flux. *Journal of Geophysical Research: Space Physics*, *89*(A7), 5625–5635.

Richards, P. G., Woods, T. N., & Peterson, W. K. (2006). Heuvac: A new high resolution solar euv proxy model. *Advances in Space Research*, *37*(2), 315–322.

Ridley, A., Deng, Y., & Toth, G. (2006). The global ionosphere–thermosphere model. *Journal of Atmospheric and Solar-Terrestrial Physics*, *68*(8), 839–864.

Rosenblatt, M. (1956). Remarks on some nonparametric estimates of a density function. *The annals of mathematical statistics*, 832–837.

Rottman, G. (2005). The sorce mission. *Solar Physics*, *230*, 7–25.

Rouillard, A., Davies, J., Lavraud, B., Forsyth, R., Savani, N., Bewsher, D., ... others (2010). Intermittent release of transients in the slow solar wind: 1. remote sensing observations. *Journal of Geophysical Research: Space Physics*, *115*(A4).

Schunk, R., & Nagy, A. (2009). *Ionospheres: physics, plasma physics, and chemistry*. Cambridge university press.

Solomon, S. C., & Qian, L. (2005). Solar extreme-ultraviolet irradiance for general circulation models. *Journal of Geophysical Research: Space Physics*, *110*(A10).

Stevenson, E., Rodriguez-Fernandez, V., Minisci, E., & Camacho, D. (2022). A deep learning approach to solar radio flux forecasting. *Acta Astronautica*, *193*, 595–606.

Sullivan, T. J. (2015). *Introduction to uncertainty quantification* (Vol. 63). Springer.

Tapping, K. (2013). The 10.7 cm solar radio flux (f10. 7). *Space weather*, *11*(7), 394–406.

Thiemann, E. M. B., Eparvier, F. A., Woodraska, D., Chamberlin, P. C., Machol, J., Eden, T., ... Woods, T. N. (2019). The goes-r euvs model for euv irradiance variability. *Journal of Space Weather and Space Climate*, *9*. doi: 10.1051/swsc/2019041

Tobiska, W. K., Woods, T., Eparvier, F., Viereck, R., Floyd, L., Bouwer, D., ... White, O. (2000). The solar2000 empirical solar irradiance model and forecast tool. *Journal of Atmospheric and Solar-Terrestrial Physics*, *62*(14), 1233–1250.

Viereck, R. A., Floyd, L. E., Crane, P. C., Woods, T. N., Knapp, B. G., Rottman, G., ... DeLand, M. T. (2004). A composite mg ii index spanning from 1978 to

This article is protected by copyright. All rights reserved.

2003. *Space Weather*, *2*(10).
Vourlidas, A., & Bruinsma, S. (2018). Euv irradiance inputs to thermospheric density models: Open issues and path forward. *Space Weather*, *16*(1), 5–15.
Warren, H. P. (2006). Nrleuv 2: A new model of solar euv irradiance variability. *Advances in Space Research*, *37*(2), 359–365.
Warren, H. P., Emmert, J. T., & Crump, N. A. (2017). Linear forecasting of the f 10.7 proxy for solar activity. *Space Weather*, *15*(8), 1039–1051.
Waskom, M. L. (2021). seaborn: statistical data visualization. *Journal of Open Source Software*, *6*(60), 3021. Retrieved from `https://doi.org/10.21105/joss.03021` doi: 10.21105/joss.03021
Woodraska, D. L., Woods, T. N., & Eparvier, F. G. (2004). In-flight calibration and performance of the solar extreme ultraviolet experiment (see) aboard the timed satellite. In *Instruments, science, and methods for geospace and planetary remote sensing* (Vol. 5660, pp. 36–47).
Woods, T. N., Bailey, S., Eparvier, F., Lawrence, G., Lean, J., McClintock, B., ... others (2000). Timed solar euv experiment. *Physics and Chemistry of the Earth, Part C: Solar, Terrestrial & Planetary Science*, *25*(5-6), 393–396.
Woods, T. N., Eparvier, F., Hock, R., Jones, A., Woodraska, D., Judge, D., ... others (2012). Extreme ultraviolet variability experiment (eve) on the solar dynamics observatory (sdo): Overview of science objectives, instrument design, data products, and model developments. *The solar dynamics observatory*, 115–143.
Woods, T. N., & Rottman, G. (2005). Xuv photometer system (xps): Solar variations during the sorce mission. *Solar Physics*, *230*, 375–387.
Young, P. R. (2021). Future prospects for solar euv and soft x-ray spectroscopy missions. *Frontiers in Astronomy and Space Sciences*, *8*, 662790.
Zhan, W., Doostan, A., Sutton, E., & Fang, T.-W. (2024). Quantifying uncertainties in the quiet-time ionosphere-thermosphere using wam-ipe. *Space Weather*, *22*(2), e2023SW003665.
Zhang, J. (2021). Modern monte carlo methods for efficient uncertainty quantification and propagation: A survey. *Wiley Interdisciplinary Reviews: Computational Statistics*, *13*(5), e1539.
Zherebtsov, G., Kovalenko, V., & Molodykh, S. (1997). Heliospheric characteristics during fast global variations of solar magnetic fields. *Journal of Geophysical Research: Space Physics*, *102*(A2), 2137–2145.

This article is protected by copyright. All rights reserved.

Author Manuscript